The Astrophysical Journal Letters, 741:L38 (5pp), 2011 November 10 doi:10.1088/2041-8205/741/2/L38


# WATER VAPOR EMISSION REVEALS A HIGHLY OBSCURED, STAR-FORMING NUCLEAR REGION IN THE QSO HOST GALAXY APM 08279+5255 AT $z = 3.9$

Paul P. van der Werf[1,2], A. Berciano Alba[1,3], M. Spaans[4], A. F. Loenen[1], R. Meijerink[1], D. A. Riechers[5], P. Cox[6], A. Weiß[7], and F. Walter[8]

[1] Leiden Observatory, Leiden University, P.O. Box 9513, NL-2300 RA Leiden, The Netherlands
[2] SUPA, Institute of Astronomy, University of Edinburgh, Royal Observatory, Blackford Hill, Edinburgh EH9 3HJ, UK
[3] ASTRON, P.O. Box 2, NL-2990 AA Dwingeloo, The Netherlands
[4] Kapteyn Astronomical Institute, University of Groningen, P.O. Box 800, NL-9700 AV Groningen, The Netherlands
[5] Astronomy Department, California Institute of Technology, MC 249-17, 1200 East California Boulevard, Pasadena, CA 91125, USA
[6] IRAM, 300 Rue de la Piscine, 38406 St. Martin d'Heres, Grenoble, France
[7] Max-Planck-Institut für Radioastronomie, Auf dem Hügel 16, Bonn, D-53121, Germany
[8] Max-Planck-Institut für Astronomie, Königstuhl 17, Heidelberg, D-69117, Germany
*Received 2011 June 23; accepted 2011 September 2; published 2011 October 21*

## ABSTRACT

We present the detection of four rotational emission lines of water vapor, from energy levels $E_u/k = 101$–$454$ K, in the gravitationally lensed $z = 3.9$ QSO host galaxy APM 08279+5255. While the lowest $H_2O$ lines are collisionally excited in clumps of warm, dense gas (density of hydrogen nuclei $n_H = (3.1 \pm 1.2) \times 10^6$ cm$^{-3}$, gas temperature $T_g \sim 105 \pm 21$ K), we find that the excitation of the higher lines is dominated by the intense local infrared radiation field. Since only collisionally excited emission contributes to gas cooling, we conclude that $H_2O$ is not a significant coolant of the warm molecular gas. Our excitation model requires the radiatively excited gas to be located in an extended region of high 100 $\mu$m opacity ($\tau_{100} = 0.9 \pm 0.2$). Locally, such extended infrared-opaque regions are found only in the nuclei of ultraluminous infrared galaxies. We propose a model where the infrared-opaque circumnuclear cloud, which is penetrated by the X-ray radiation field of the QSO nucleus, contains clumps of massive star formation where the $H_2O$ emission originates. The radiation pressure from the intense local infrared radiation field exceeds the thermal gas pressure by about an order of magnitude, suggesting close to Eddington-limited star formation in these clumps.

*Key words:* galaxies: ISM – galaxies: nuclei – quasars: individual (APM 08279+5255)

*Online-only material:* color figures

## 1. INTRODUCTION

Water is expected to be one of the most abundant molecules in molecular clouds in galaxies. In cold molecular clouds, water is in the form of icy mantles on dust grains, with total $H_2O$ abundances up to $10^{-4}$ with respect to hydrogen nuclei (Tielens et al. 1991), thus containing up to 30% of the available oxygen atoms. In warm molecular clouds, such as in star-forming galaxies or galaxies with a luminous active galactic nucleus, water can evaporate from the dust grains when the grain temperature becomes sufficiently high. $H_2O$ molecules can also be released into the gas phase by photodesorption in regions exposed to ultraviolet (UV) radiation and by desorption induced by cosmic rays or X-rays in more obscured regions (Hollenbach et al. 2009), or by sputtering of grains in shocks. In warm molecular gas, $H_2O$ can also be formed in the gas phase, through ion–neutral chemistry in regions with a sufficiently high fractional ionization, or through neutral–neutral chemistry in regions sufficiently warm that the relevant activation energy barriers can be overcome. Gas-phase $H_2O$ may play an important role as a cooling agent of warm, dense molecular clouds (Neufeld & Kaufman 1993; Neufeld et al. 1995). The large Einstein $A$-values of $H_2O$ rotational transitions lead to high critical densities ($\gtrsim 10^8$ cm$^{-3}$) so that collisional excitation will only be effective in very dense gas.

Due to the wet Earth atmosphere, bulk gas-phase water can only be detected from space or from distant objects where the cosmological redshift moves the $H_2O$ lines into transparent atmospheric windows. Despite the detection of a 22 GHz water maser in a $z = 2.6$ QSO (Impellizzeri et al. 2008), previous searches for non-maser rotational emission lines of $H_2O$ from high-$z$ objects remained unsuccessful (Wagg et al. 2006; Riechers et al. 2006, 2009b), until the recent detection of the $2_{0,2} - 1_{1,1}$ $H_2O$ emission line from a gravitationally lensed galaxy at $z = 2.3$ (Omont et al. 2011). However, neither the molecular excitation mechanism nor the water abundance could be derived on the basis of the detection of a single optically thick line.

The *Herschel Space Observatory* has recently enabled the first detections of $H_2O$ emission lines from two nearby galaxies, with very different results between the two objects (Van der Werf et al. 2010; González-Alfonso et al. 2010; Weiß et al. 2010). Spectra of the lowest $H_2O$ transitions in the nearby starburst galaxy M82 revealed faint lines with complex spectral shapes, with one of the lines (the $1_{1,1}$–$0_{0,0}$ para-$H_2O$ ground-state line) in absorption (Weiß et al. 2010). No $H_2O$ emission from higher rotational levels was found (Panuzzo et al. 2010). In marked contrast, observations of the nearby ultraluminous infrared galaxy (ULIRG) and QSO Mrk 231 revealed a rich spectrum of $H_2O$ lines from upper level energies $E_u$ up to $E_u/k = 640$ K (where $k$ is the Boltzmann constant), whereas the lower lines connecting to the ground state remained undetected (Van der Werf et al. 2010).

In order to search for $H_2O$ in a high-$z$ galaxy in a systematic way, we undertook a search for four lines of $H_2O$ in the gas-rich $z = 3.9$ QSO host galaxy APM 08279 + 5255 (Irwin et al. 1998; Lewis et al. 1998). This object is gravitationally lensed with a magnification factor $\mu = 4$ according to the model of Riechers

**Table 1**
Parameters of $H_2O$ Line Emission from APM 08279+5255

| Transition | $2_{0,2}$–$1_{1,1}$ | $2_{1,1} - 2_{0,2}$ | $3_{2,1} - 3_{1,2}$ | $4_{2,2} - 4_{1,3}$ | $1_{1,0} - 1_{0,1}$ | |
|---|---|---|---|---|---|---|
| $\nu_0$[a] | 987.926 | 752.033 | 1162.911 | 1207.638 | 556.936 | GHz |
| $\nu_{obs}$[b] | 201.166 | 153.132 | 236.797 | 245.905 | | GHz |
| $E_u/k$[c] | 101 | 137 | 305 | 454 | 61 | K |
| Flux density calibrator | 3C273 | 3C84 | 3C273 | 0923+392 | | |
| and flux density[d] | 8.0 | 8.5 | 7.3 | 4.3 | | Jy |
| Synthesized beam[e] | 0.″58 × 0.″60, 33° | 2.″98 × 1.″87, 47° | 0.″62 × 0.″56, 48° | 0.″61 × 0.″44, 49° | | |
| $\sigma$[f] | 2.5 | 1.7 | 7.1 | 4.3 | | mJy |
| $S_{cont}$[g] | $16.5 \pm 0.8$ | $5.4 \pm 0.3$ | $26.6 \pm 1.3$ | $31.4 \pm 2.0$ | | mJy |
| $I_{line}$[h] | $9.1 \pm 0.9$ | $4.3 \pm 0.6$ | $8.0 \pm 0.9$ | $7.5 \pm 2.1$ | <0.7[n] | Jy km s$^{-1}$ |
| $I_{model}$[i] | 8.9 | 4.5 | 8.4 | 6.5 | 0.25 | Jy km s$^{-1}$ |
| $v_0$[j] | $72 \pm 35$ | $47 \pm 25$ | $93 \pm 16$ | $50 \pm 43$ | | km s$^{-1}$ |
| FWHM[k] | $492 \pm 84$ | $480 \pm 58$ | $312 \pm 37$ | $429 \pm 96$ | | km s$^{-1}$ |
| $L'_{line}$[l,m] | $(7.9 \pm 0.8) \times 10^{10}$ | $(6.5 \pm 1.0) \times 10^{10}$ | $(5.1 \pm 0.5) \times 10^{10}$ | $(4.5 \pm 1.3) \times 10^{10}$ | $<1.9 \times 10^{10}$ | K km s$^{-1}$ pc$^2$ |
| $L_{line}$[l,m] | $(2.4 \pm 0.5) \times 10^9$ | $(8.9 \pm 1.3) \times 10^8$ | $(2.6 \pm 0.3) \times 10^9$ | $(2.6 \pm 0.7) \times 10^9$ | $<1.1 \times 10^8$ | $L_\odot$ |

**Notes.**
[a] Rest frequency of the line.
[b] Observing frequency.
[c] Upper level energy of the transition.
[d] Assumed flux density of flux calibrator at observing frequency.
[e] Full width at half-maximum and position angle.
[f] rms noise in the integrated spectrum at $\Delta v = 40$ MHz.
[g] Observed integrated continuum flux density.
[h] Observed integrated line flux.
[i] Modeled integrated line flux.
[j] Center velocity of fitted Gaussian relative to $z = 3.911$.
[k] Full width at half-maximum of fitted Gaussian.
[l] Using $z = 3.911$, $H_0 = 70$ km s$^{-1}$ Mpc$^{-1}$, $\Omega_\Lambda = 0.73$, and $\Omega_{tot} = 1$.
[m] Not corrected for lensing.
[n] Upper limit from Wagg et al. (2006).

et al. (2009b). With CO lines detected from rotational levels up to $J = 11$ (Weiß et al. 2007; Riechers et al. 2009a) and HCN, HNC, and $HCO^+$ lines from levels up to $J = 6$ (Wagg et al. 2005; García-Burillo et al. 2006; Riechers et al. 2010), its molecular medium has been characterized very well. Analysis of the CO rotational ladder revealed unusually high excitation (Weiß et al. 2007). However, a previous search for the ortho ground-state $1_{1,0}$–$1_{0,1}$ $H_2O$ line (upper level energy $E_u/k = 61$ K) was unsuccessful (Wagg et al. 2006). We therefore targeted lines of higher excitation, with $E_u/k$ from 101 to 454 K.

## 2. OBSERVATIONS AND RESULTS

We used the Institut de Radioastronomie Millimétrique (IRAM) Plateau de Bure Interferometer (Guilloteau et al. 1992) with six antennas in 2010 December and 2011 February to observe the four $H_2O$ lines listed in Table 1 (which also lists all relevant observational parameters) in APM 08279+5255. Observing times (including overheads) varied from 2 to 5.2 hr per line. The WIDEX back end was used, providing 3.6 GHz instantaneous bandwidth in dual polarization. Data reduction using the GILDAS package included the standard steps of data flagging, amplitude, phase and bandpass calibration, and conversion into datacubes. The flux density scale is accurate to within 15%. The datacubes were deconvolved using a CLEAN algorithm (Clark 1980).

All four lines were detected and an image of the flux distribution of the $2_{1,1} - 2_{0,2}$ line is shown in Figure 1. Fits to the continuum $uv$-data were used to calculate the continuum fluxes (reported in Table 1) and source sizes. In the high angular resolution observations the emission was found to be slightly

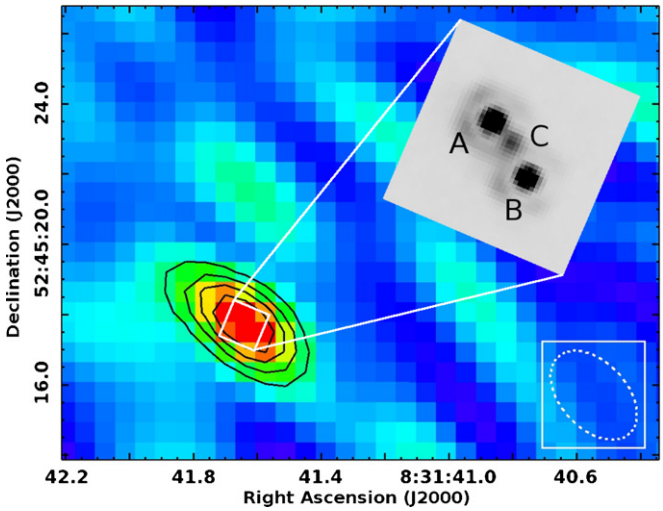


**Figure 1.** $H_2O$ emission from APM 08279+5255. The contoured pseudocolor map shows the distribution of the velocity-integrated continuum-subtracted $H_2O$ $2_{1,1} - 2_{0,2}$ line flux, with contour levels of $3\sigma$, $5\sigma$, $7\sigma$, and $9\sigma$, where $\sigma = 0.5$ Jy km s$^{-1}$ beam$^{-1}$. The dashed white ellipse indicates the synthesized beam. The inset presents the NICMOS F110W image (Ibata et al. 1999) and shows that the gravitationally lensed images (the brightest of which are 0.″378 apart) are fully covered by the synthesized beam.
(A color version of this figure is available in the online journal.)

spatially resolved, with source sizes of approximately 0.″5, in agreement with high-resolution observations of the 1 mm continuum (Krips et al. 2007), and CO 1–0 (Riechers et al. 2009b). Integrated spectra of the four $H_2O$ lines are shown in Figure 2 and parameters of the detected lines are presented in

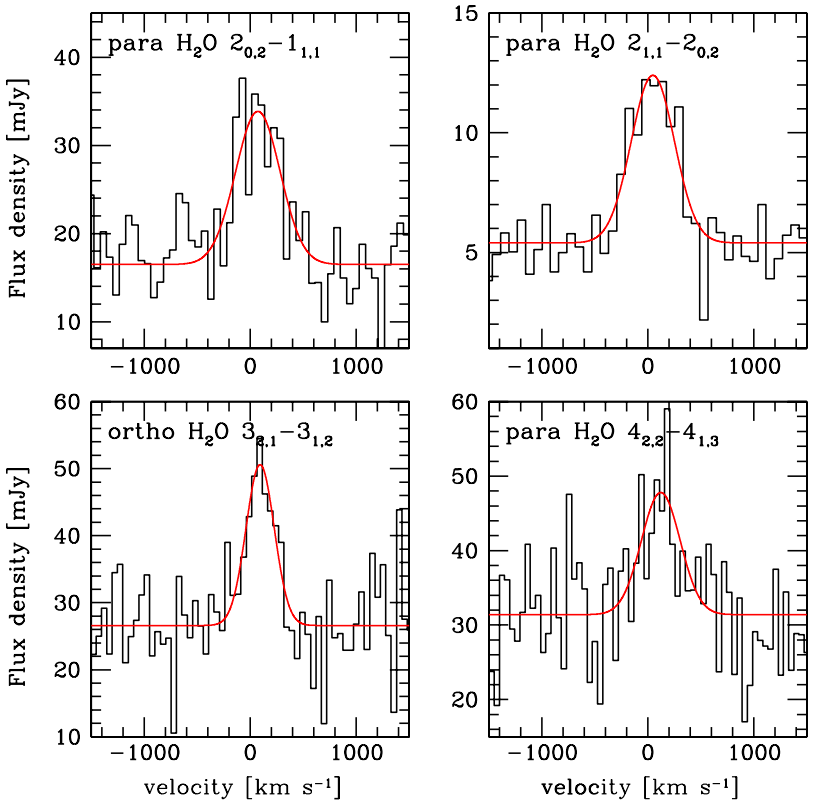


**Figure 2.** Spectra of $H_2O$ emission lines from APM 08279+5255 at a common frequency resolution of 40 MHz. The horizontal axis shows velocity relative to redshift $z = 3.911$. The red curves indicate Gaussian fits to each spectrum.

(A color version of this figure is available in the online journal.)

Table 1. The most sensitive detection is that of the $2_{1,1} - 2_{0,2}$ line, which displays a symmetric line profile with a full width at half-maximum (FWHM) of $480 \pm 58$ km s$^{-1}$, excellently matching the FWHM values of 445–520 km s$^{-1}$ of the CO lines (Weiß et al. 2007). Recently, a low spectral resolution 1 mm spectrum of APM 081279+5255 obtained with Z-Spec has been released by Bradford et al. (2011). In the Z-Spec spectrum, the $3_{2,1} - 3_{1,2}$ line is the only $H_2O$ line detected at the $3\sigma$ level, but our flux measurement for this line is a factor two lower. This discrepancy is similar to that between the CO line fluxes measured by Z-Spec and by the IRAM 30 m telescope, several of which have been independently confirmed by the IRAM Plateau de Bure Interferometer (Weiß et al. 2007). A similar discrepancy is found between our flux measurement of the $4_{2,2} - 4_{1,3}$ line and that by Bradford et al. (2011), although the latter had a significance of only $2.5\sigma$. The continuum flux densities match very well between the two data sets. Finally, we note that the serendipitous detection of another $H_2O$ line, the $2_{2,0} - 2_{1,1}$ line, using the IRAM Plateau de Bure Interferometer, was recently reported by Lis et al. (2011).

## 3. FAR-IR PUMPED $H_2O$ EMISSION

The distribution of the detected line flux as a function of the energy of the upper level of the transition is shown in Figure 3. The flux distribution shows considerable emission out to the $4_{2,2} - 4_{1,3}$ line, implying that for purely collisional excitation the kinetic temperature must be of the order of at least 400 K. Critical densities are approximately $10^8$ cm$^{-3}$ for the lowest lines ($2_{0,2} - 1_{1,1}$ and $2_{1,1} - 2_{0,2}$) and higher than $10^8$ cm$^{-3}$ for the higher lines. Therefore, any purely collisionally excited model that can account for the observed $3_{2,1} - 3_{1,2}$ and $4_{2,2} - 4_{1,3}$ fluxes would produce much stronger emission in the lower lines, including the $1_{1,0} - 1_{0,1}$ level, for which a sensitive upper limit exists (Wagg et al. 2006). We therefore rule out purely collisional

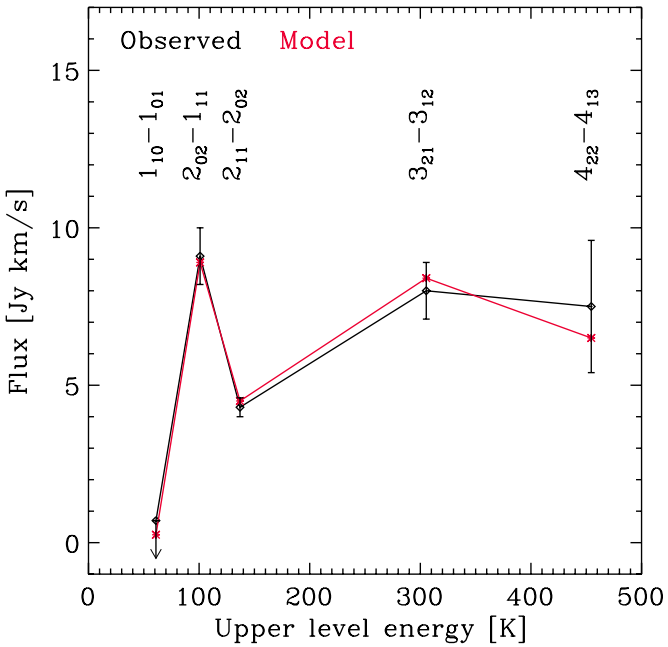


**Figure 3.** Flux in $H_2O$ emission lines from APM 08279+5255 as a function of upper level energy $E_u$. Black symbols and error bars indicate the observed line fluxes and the previously published upper limit on $1_{1,0} - 1_{0,1}$ (indicated by a downward arrow). Red crosses indicate values produced by our model as described in the text.

(A color version of this figure is available in the online journal.)

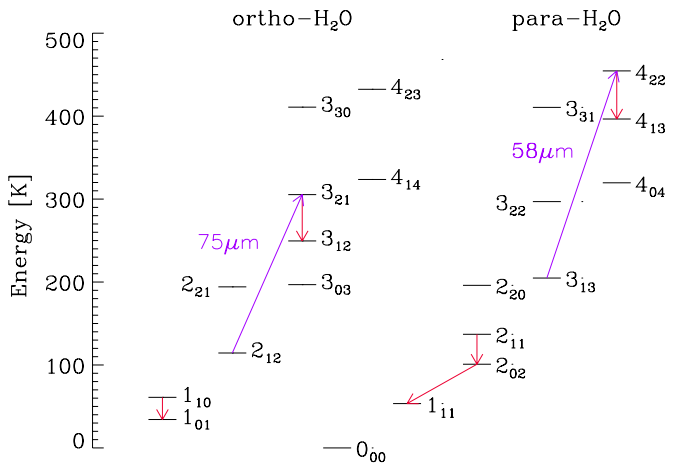


**Figure 4.** Partial $H_2O$ energy level diagram. The ortho- and para-$H_2O$ rotational ladders are indicated, and the transitions detected here as well as the upper limit on the $1_{1,0}-1_{0,1}$ ortho-$H_2O$ ground-state transition are indicated by red arrows. Purple arrows indicate the radiative pumping transitions at 58 and 75 $\mu$m that account for the efficient population of the $4_{2,2}$ and $3_{2,1}$ levels.

(A color version of this figure is available in the online journal.)

excitation and consider in addition radiative excitation by an intense far-infrared (far-IR) radiation field from warm dust, with a temperature $T_d = 220$ K, as derived from the continuum spectral energy distribution (Weiß et al. 2007; Riechers et al. 2009b).

We model these coupled processes using a radiative transfer code (Poelman & Spaans 2005, 2006) which computes the statistical equilibrium populations of all relevant $H_2O$ levels in the ground and first vibrationally excited state. Line radiation is transferred in a non-local and three-dimensional manner through a multi-zone escape probability calculation. The model consists of dense clumps within a spherical region with a radius of 100 pc. Due to the high critical densities of the $H_2O$ lines, only the clumps contribute to the $H_2O$ emission, and we have run a model grid where we varied gas temperatures over the range $T_g = 50$–$200$ K and $H_2O$ column densities over $10^{16}$–$10^{18}$ cm$^{-2}$. Clump densities were varied only over the range $n_H = 10^5$–$10^7$ cm$^{-3}$, since higher densities ($\sim 10^8$ cm$^{-3}$) would produce low rotational lines ($2_{1,1}-2_{0,2}$ and $2_{0,2}-1_{1,1}$) much stronger than $3_{2,1}-3_{1,2}$, contrary to what is observed. The $H_2O$ ortho-to-para ratio was obtained from thermal equilibrium (Poelman & Spaans 2005) and found to be very close to the statistical equilibrium value of 3. We fixed the gas-to-dust mass ratio at 100, and the local turbulent velocity dispersion at 4 km s$^{-1}$, with a total velocity difference (gradient times length) across the model region of 140 km s$^{-1}$.

In our best-fit model, the clumps have a density of hydrogen nuclei $n_H = (3.1 \pm 1.2) \times 10^6$ cm$^{-3}$, a gas temperature $T_g = 105 \pm 21$ K, and the average density of hydrogen nuclei over the 100 pc radius model region is $\langle n_H \rangle = 4000 \pm 1000$ cm$^{-3}$, yielding a 100 $\mu$m continuum optical depth $\tau_{100} \approx 0.9 \pm 0.2$. The line fluxes predicted by the best-fit model are listed in Table 1 and shown in Figure 3. The lowest lines (up to $2_{1,1}-2_{0,2}$) are excited mostly by collisions. The clump density and temperature derived in our model are determined by these lines, and the required density is somewhat higher than that derived from the CO lines (Weiß et al. 2007), which is not surprising given the higher critical densities of the $H_2O$ lines. In contrast, the $4_{2,2}$ and $3_{2,1}$ levels are populated exclusively by the absorption of far-IR photons. As shown in Figure 4, the pumping occurs at 58 and 75 $\mu$m rest-frame wavelengths. The intensity of the radiatively excited lines provides a measure of the intensity of the local far-IR radiation field and therefore of the optical depth in the spectral region of the pumping wavelengths, and this determines the 100 $\mu$m optical depth in our model. The relative strengths of the $4_{2,2}-4_{1,3}$ and $3_{2,1}-3_{1,2}$ lines in principle provide information on the color temperature of the far-IR radiation field, but for $T_d > 100$ K the pumping wavelengths are on the Rayleigh–Jeans tail of the warm dust continuum, making the line ratio insensitive to the dust temperature. Since only collisionally excited lines contribute to the cooling (i.e., removal of kinetic energy) of warm molecular gas, we find that cooling by the $H_2O$ lines is unimportant compared to the cooling by CO rotational lines, in contrast to the conclusion by Bradford et al. (2011) and to earlier theoretical suggestions (Neufeld & Kaufman 1993; Neufeld et al. 1995). We note that radiative excitation has also been suggested to drive the intensity of HCN lines in APM 08279+5255 (García-Burillo et al. 2006; Weiß et al. 2007). Furthermore, the upper levels of the [C II] 158 $\mu$m line and the [Si II] 35 $\mu$m line are also affected by radiative pumping, as shown by rest-frame UV absorption line measurements by Srianand & Petitjean (2000), who conclude that the absorbing clouds must be located closer to the extended (>200 pc) source of far-IR radiation than to the UV source.

In our best-fit model, the $4_{2,2}-4_{1,3}$ line is only moderately optically thick (optical depth approximately 1.7), and is thus sensitive to the total column density of warm ($T_g > 100$ K) water vapor in our model region (unlike the other lines, which have line center optical depths from 30 to 300). We find a total (beam-averaged) warm $H_2O$ column density of $2.6 \times 10^{17}$ cm$^{-2}$, i.e., a warm $H_2O/H_2$ abundance of approximately $6 \times 10^{-7}$, consistent with UV or X-ray irradiated chemical models (Meijerink & Spaans 2005).

## 4. IMPLICATIONS FOR THE NUCLEAR REGION OF APM 08279+5255

The $H_2O$ line ratios observed in APM 08279+5255 are very different from those observed in prominent star-forming regions in the Milky Way. Water lines from UV irradiated gas (photon-dominated regions or PDRs) in the Milky Way show thermal level populations (White et al. 2010; Habart et al. 2010), dominated by low-lying lines. These lines are much fainter than CO lines in the same frequency range. The best case in point is the prominent Orion Bar PDR where only a few low lying $H_2O$ lines are detected (Habart et al. 2010), and the $2_{1,1}-2_{0,2}/1_{1,0}-1_{0,1}$ luminosity ratio is 0.6; in contrast, in APM 08279+5255, this ratio is >8.1. Furthermore, in APM 08279+5255, the $H_2O$ lines have luminosities comparable to CO lines in the same frequency range, while they are two orders of magnitude fainter in the Orion Bar (e.g., the $H_2O$ $2_{1,1}-2_{0,2}$ / CO(6−5) line luminosity ratio is 0.6 in APM 08279+5255, while it is 0.026 in the Orion Bar). The only object with properties comparable to APM 08279+5255 is the nearby ULIRG/QSO Mrk 231 (Van der Werf et al. 2010), where high $H_2O$ lines were also found to be radiatively excited (González-Alfonso et al. 2010), and the two objects show very similar $3_{2,1}-3_{1,2}/2_{0,2}-1_{1,1}$ luminosity ratios.

The fact that in the presence of an intense far-IR radiation field the most luminous $H_2O$ emission is radiatively excited follows directly from the large Einstein $A$-values of the $H_2O$ rotational lines, which result in high critical densities as well as a strong coupling to the local far-IR radiation field. A key result of our analysis is therefore the presence of a sufficiently intense local far-IR radiation field, which requires the emitting clumps

to be located in an obscured environment, with $\tau_{100} \sim 0.9$. The essential difference with the $H_2O$ excitation in the Orion Bar PDR (aside from less important differences in temperature and density) is the fact that the latter has a low 100 $\mu$m optical depth, while in APM 08279+5255 $\tau_{100} \approx 0.9$ over the entire region sampled. The minimum size of the this region follows from the blackbody limit, which is calculated by assigning the entire $L_{\rm FIR} = 5 \times 10^{13} L_\odot$ (corrected for gravitational amplification) to a blackbody with $T = 220$ K. The resulting radius is $R = 110$ pc for a spherical model or a factor of $\sqrt{2}$ larger for a disk-like configuration, as preferred by Riechers et al. (2009b). The most recent lensing model, which accurately reproduces the positions and luminosities of the gravitationally lensed images of the QSO nucleus, assigns the CO(1 − 0) emission to a disk of radius of 550 pc, at an inclination of less than 30° from face-on (Riechers et al. 2009b). Because of the excellent match of the $H_2O$ and CO line widths, it is likely that the region of $H_2O$ emission, with $T_{\rm d} = 220$ K and $\tau_{100} \sim 0.9$, has the same radius as the CO emission region.

The CO rotational line ladder of APM 08279+5255 shows even higher excitation than that of Mrk 231 and therefore most likely reveals the presence of an XDR (Weiß et al. 2007; Van der Werf et al. 2010). Since high $H_2O$ abundances can be generated in both PDRs and XDRs (Meijerink & Spaans 2005), our data do not distinguish directly between these models. However, while X-rays easily traverse and heat large column densities of gas, they are inefficient at heating the dust, and dust temperatures higher than ∼50 K are hard to achieve over extended regions (Yan 1997; Meijerink & Spaans 2005). The high dust temperature of ∼220 K over a ∼550 pc radius region is more easily achieved in PDRs, generated by widespread star formation in clumps of dense gas throughout the circumnuclear gas disk. Regions of several 100 pc radius, with high 100 $\mu$m optical depths, are locally found only in the central regions of ULIRGs (Solomon et al. 1997). The fact that in this study we find such a region in a QSO provides support for the scenario where ULIRGs form the birthplaces of QSOs (Sanders et al. 1988).

If our suggestion that the extended warm dust continuum is generated by circumnuclear star formation in APM 08279+5255 is correct, this star formation is taking place in the presence of the strong and penetrative X-ray radiation field generated by the AGN (Gallagher et al. 2002; Hasinger et al. 2002; Chartas et al. 2002). As shown by Hocuk & Spaans (2010), in this situation fragmentation is inhibited and a top-heavy stellar initial mass function is expected to result. It is possible that this effect accounts for the extraordinary far-IR luminosity $L_{\rm FIR} = 5 \times 10^{13} L_\odot$ (corrected for gravitational amplification) of APM 08279+5255. We note also that in the clumps in our model, both turbulent pressure $P_{\rm turb} \sim \rho \sigma_v^2/3$ (where $\rho$ is the mass density of the gas clump and $\sigma_v$ its turbulent velocity dispersion) and radiation pressure $P_{\rm rad} \sim \tau_{100} \sigma T_{\rm d}^4/c$ (where $\sigma$ is the Stefan-Boltzmann constant and $c$ the speed of light) exceed the thermal pressure $P_{\rm th} \sim n_{\rm H_2} k T_{\rm g}$ by a large factor. Inserting numbers from our best-fit model, we find that $P_{\rm th} \sim 3 \times 10^{-8}$ erg cm$^{-3}$, while $P_{\rm turb} \sim P_{\rm rad} \sim 3 \times 10^{-7}$ erg cm$^{-3}$. Radiation pressure therefore plays an important role in the dynamics of the circumnuclear gas cloud. If the clumps are indeed forming stars, as we are suggesting, the star formation process is then close to Eddington-limited, in agreement with the model developed by Thompson et al. (2005) for starburst regions surrounding a supermassive black hole.

Our study demonstrates how radiatively excited $H_2O$ lines can be used to reveal the presence of extended infrared-opaque regions in galactic nuclei (even without spatially resolving these regions). Furthermore, we can derive local conditions in the infrared-opaque nuclear gas disk, which in the present case indicates close to Eddington-limited star formation. While for local galaxies observations from space will remain necessary to observe the $H_2O$ lines, the Atacama Large Millimeter Array will make this diagnostic readily available in galaxies with sufficient redshift, without the aid of gravitational lensing.

This work is based on observations carried out with the IRAM Plateau de Bure Interferometer. IRAM is supported by INSU/CNRS (France), MPG (Germany) and IGN (Spain). D.R. acknowledges support from NASA through a Spitzer grant. We thank Melanie Krips for expert assistance with the IRAM data reduction and Rodrigo Ibata for providing the NICMOS image used in Figure 1. We also thank Xander Tielens for commenting on an earlier version of this Letter.

*Facility:* IRAM:Interferometer

## REFERENCES

Bradford, C. M., Bolatto, A. D., Maloney, P. R., et al. 2011, ApJ, 741, L37
Chartas, G., Brandt, W. N., Gallagher, S. C., & Garmire, G. P. 2002, ApJ, 579, 169
Clark, B. G. 1980, A&A, 89, 377
Gallagher, S. C., Brandt, W. N., Chartas, G., & Garmire, G. P. 2002, ApJ, 567, 37
García-Burillo, S., Graciá-Carpio, J., Guélin, M., et al. 2006, ApJ, 645, L17
González-Alfonso, E., Fischer, J., Isaak, K., et al. 2010, A&A, 518, L43
Guilloteau, S., Delannoy, J., Downes, D., et al. 1992, A&A, 262, 624
Habart, E., Dartois, E., Abergel, A., et al. 2010, A&A, 518, L116
Hasinger, G., Schartel, N., & Komossa, S. 2002, ApJ, 573, L77
Hocuk, S., & Spaans, M. 2010, A&A, 522, A24
Hollenbach, D., Kaufman, M. J., Bergin, E. A., & Melnick, G. J. 2009, ApJ, 690, 1497
Ibata, R. A., Lewis, G. F., Irwin, M. J., Lehár, J., & Totten, E. J. 1999, AJ, 118, 1922
Impellizzeri, C. M. V., McKean, J. P., Castangia, P., et al. 2008, Nature, 456, 927
Irwin, M. J., Ibata, R. A., Lewis, G. F., & Totten, E. J. 1998, ApJ, 505, 529
Krips, M., Peck, A. B., Sakamoto, K., et al. 2007, ApJ, 671, L5
Lewis, G. F., Chapman, S. C., Ibata, R. A., Irwin, M. J., & Totten, E. J. 1998, ApJ, 505, L1
Lis, D. C., Neufeld, D. A., Phillips, T. G., Gerin, M., & Neri, R. 2011, ApJ, 738, L6
Meijerink, R., & Spaans, M. 2005, A&A, 436, 397
Neufeld, D. A., & Kaufman, M. J. 1993, ApJ, 418, 263
Neufeld, D. A., Lepp, S., & Melnick, G. J. 1995, ApJS, 100, 132
Omont, A., Neri, R., Cox, P., et al. 2011, A&A, 530, L3
Panuzzo, P., Rangwala, N., Rykala, A., et al. 2010, A&A, 518, L37
Poelman, D. R., & Spaans, M. 2005, A&A, 440, 559
Poelman, D. R., & Spaans, M. 2006, A&A, 453, 615
Riechers, D. A., Walter, F., Bertoldi, F., et al. 2009a, ApJ, 703, 1338
Riechers, D. A., Walter, F., Carilli, C. L., & Lewis, G. F. 2009b, ApJ, 690, 463
Riechers, D. A., Weiß, A., Walter, F., Carilli, C. L., & Knudsen, K. K. 2006, ApJ, 649, 635
Riechers, D. A., Weiß, A., Walter, F., & Wagg, J. 2010, ApJ, 725, 1032
Sanders, D. B., Soifer, B. T., Elias, J. H., et al. 1988, ApJ, 325, 74
Solomon, P. M., Downes, D., Radford, S. J. E., & Barrett, J. W. 1997, ApJ, 478, 144
Srianand, R., & Petitjean, P. 2000, A&A, 357, 414
Thompson, T. A., Quataert, E., & Murray, N. 2005, ApJ, 630, 167
Tielens, A. G. G. M., Tokunaga, A. T., Geballe, T. R., & Baas, F. 1991, ApJ, 381, 181
Van der Werf, P. P., Isaak, K. G., Meijerink, R., et al. 2010, A&A, 518, L42
Wagg, J., Wilner, D. J., Neri, R., Downes, D., & Wiklind, T. 2005, ApJ, 634, L13
Wagg, J., Wilner, D. J., Neri, R., Downes, D., & Wiklind, T. 2006, ApJ, 651, 46
Weiß, A., Downes, D., Neri, R., et al. 2007, A&A, 467, 955
Weiß, A., Requena-Torres, M. A., Güsten, R., et al. 2010, A&A, 521, L1
White, G. J., Abergel, A., Spencer, L., et al. 2010, A&A, 518, L114
Yan, M. 1997, PhD thesis, Harvard Univ.